Tuning and understanding the electronic effect of Co-Mo-O sties in bifunctional electrocatalysts for ultralong-lasting rechargable zinc-air battery

Yi Guan[1,§], Nan Li[1,§], Jiao He[1], Yongliang Li[1]*, Lei Zhang[1], Qianling Zhang[1], Xiangzhong Ren[1]*, Chuanxin He [1], LiRong Zheng [2], Xueliang Sun [3]

[1] College of Chemistry and Environmental Engineering, Shenzhen University, Shenzhen, Guangdong 518060, P.R. China

[2] Institute of High Energy Physics Chinese Academy of Sciences, Beijing 100049, P.R. China

[3] Department of Mechanical and Materials Engineering, University of Western Ontario, London, Ontario, N6A 6B9, Canada

[§]Yi Guan and Nan Li contributed equally to this work.

[*] Corresponding authors: Xiangzhong Ren, Email: renxz@szu.edu.cn, Tel/Fax: +86-755-26558134; Yongliang Li, Email: liyli@szu.edu.cn, Tel/Fax: +86-755-26931162

Chemicals

Molybdenum trioxide (MoO_3;≥99.0%), Imidazole ($C_3H_4N_2$; ≥99.0% Zinc acetate ($Zn(Ac)_2$; ≥99.0%), Cobalt acetate ($Co(Ac)_2$; ≥99.0%), 2-methylimidazole (2-mIm; 98.0%), Polyvinylpyrrolidone (PVP, K29-32), All the chemicals were purchased from Aladdin Industrial Corporation. and used as received without further purification.

Experimental Section

Synthesis of Mo-MOF: Mo-MOF was modified according to the preparation process previously reported. [1] Firstly, 0.068 g imidazole and 0.144 g MoO_3 were mixed in 100 mL specific solvent (the composition of the solution is methanol and water in a volume ratio of 3:2). Then after stirred for 12 hours, the product has been centrifuged three times at 10000 rpm to obtain a precipitate.

Synthesis of Mo-MOF @ BIMZIF: Dissolve 1 g of PVP and 30 mg of Mo-MOF in 25 mL of water to obtain solution A. Dissolve 1.5 mmol of a mixture of cobalt acetate and zinc acetate in 20 mL of water to obtain solution B. Mix A and B solutions to obtain solution C. 2.63 g of dimethylimidazole was dissolved in 25 mL of water to obtain solution D. Solution D was added dropwise to C and stirred for 12h to obtain Mo-

MOF@BIMZIF.

Synthesis of Co-MoO_2-NC products: The prepared Mo-MOF @ BIMZIF first undergoes a pyrolysis process at 400°C for 1 h, and then continues the second heating process at 800/900/1000°C for 2 h. The above pyrolysis process is carried out in a nitrogen atmosphere at a heating rate of 5 degrees per minute. The final products are Co-MoO_2-NC-800/900/1000.

Preparation of the Working Electrode

The catalyst ink was prepared by ultrasonically dispersing 5 mg samples in a mixture of 1.5 mL ethanol and 40 μL dilute aqueous Nafion solution (5 wt% solution in a mixture of lower aliphatic alcohols and DuPont water). The working electrode was obtained by ultrasonically dispersing and dropping 15 μL catalyst ink on a glassy carbon RRDE (with a disk diameter of 4 mm, A_{disk}= 0.126 cm^2; inner/outer-ring diameter: 5.0/7.0 mm, A_{ring} = 0.188 cm^2) from BAS Inc. The catalyst loading was all 0.398 mg cm^{-2} based on the geometric electrode area of 0.126 cm^2. The state-of-the-art commercial Pt/C and Ir/C were mechanically mixed (mass ratio = 1:1) as the reference.

Material characterization

The crystallite structure was investigated by powder X-ray diffraction pattern (PXRD) on a PANalytical/Empyrean with Cu Kα radiation. The morphology and microstructure were inspected using a field emission scanning electron microscope (FESEM, JEOL JSM-7800F) and transmission electron microscopy (TEM, JEOL-F200), respectively. X-ray photoelectron spectroscopy (XPS) measurements were performed on a K-Alpha+ using a monochromic Al X-ray source. Raman spectra were obtained using a Renishaw/INVIA REFLEX spectrometer coupled with a 633 nm laser. Nitrogen adsorption-desorption isotherms were measured using a BELSORP-max. The specific surface area and pore size distribution were determined using the Brunauer-Emmett-Teller (BET) theory and the nonlocal density functional theory (NLDFT) method, respectively.

X-ray absorption fine structure measurements: The X-ray absorption fine structure (XAFS) spectra were collected at the 1W1B station at the Beijing Synchrotron Radiation Facility (BSRF). The storage rings of BSRF operated at 2.5 GeV with a maximum current of 250 mA. Using a silicon (Si) (111) double-crystal monochromator,

the data collection was carried out in the transmission mode using an ionization chamber. All spectra were collected in ambient conditions. The acquired extended XAFS (EXAFS) data were processed according to the standard procedures, using the Athena module implemented in the IFEFFIT software package. The k^3-weighted EXAFS spectra were obtained by subtracting the post-edge background from the overall absorption, followed by normalization with respect to the edge-jump step. Subsequently, k^3-weighted $\chi(k)$ data of the Cu K-edge were Fourier transformed to real (R) space, using a Hanning window (dk = 1.0 $Å^{-1}$) to separate the EXAFS contributions from different coordination shells. To obtain thequantitative structural parameters around central atoms, least-squares curve parameter fitting was performed using the Artemis module of the IFEFFIT software package.

Electrochemical Evaluations

The electrochemical measurements were conducted on a three-electrode system with an CHI760E electrochemical workstation which assembled with an MSR electrode rotator (BAS RRDE-3A). A three-electrode cell was used to perform the electrochemical measurements. Ag/AgCl (saturated KCl) was used as reference electrode. The carbon rod was used as a counter electrode. All potential values refer to that of a reversible hydrogen electrode (RHE). The potential, measured against a Ag/AgCl electrode, was converted to a potential versus RHE according to $E_{(vs.RHE)} = E_{(vs.Ag/AgCl)}+0.197+0.059pH$. All electrochemical measurements were carried out at 25 °C. The ORR/OER evaluation was performed in electrolyte saturated and protected by bubbling O_2 for at least 30 min. The scan rate for ORR/OER measurements was 5 mV s^{-1}. The ORR polarization curves were collected at various rotation rates ranging from 625 to 2025 rpm for calculating the electron transfer number. The accelerated durability tests were performed at room temperature in oxygen-saturated 0.1 M KOH solution at a sweep rate of 100 mV s^{-1} for 2000 cycles from 0.2 V to -0.8 V. The i-t chronoamperometric response was conducted in oxygen-saturated 0.1 M KOH solution at 0.465 V versus RHE for 22500s for the ORR. The electron transfer number (n) can be determined using Koutecky–Levich (K–L) equations as given by:

$$\frac{1}{J} = \frac{1}{B\omega^{1/2}} + \frac{1}{J_K} \quad (1)$$

in which

$$B = 0.2nFC_0\ (D_0)^{2/3} v^{-1/6} \quad (2)$$

$$J_K = nFkC_0 \quad (3)$$

where J is the measured current density, J_K is the kinetic current densities, ω is the angular velocity of the disk (ω = 2πN where N is the linear rotation speed), and n is the overall number of electrons transferred in oxygen reduction. F is the Faraday constant (F = 96485 C mol^{-1}), C_0 is the bulk concentration of O_2, ν is the kinematic viscosity of the electrolyte, k is the electron transfer rate constant, and D_0 is the diffusion coefficient of O_2 in the electrolyte. The constant 0.2 is adopted when the rotating speed is expressed in rpm.

The electron transfer number (n) and the corresponding peroxide yield (HO^{2-}% in alkaline solution) can also be determined on the basis of the disk and ring currents using the following equations:

$$n = 4 \times \frac{I_{disk}}{I_{disk} + I_{ring} / N} \quad (4)$$

$$peroxide\% = 100 \times \frac{2I_{ring} / N}{I_{disk} + I_{ring} / N} \quad (5)$$

where I_{disk} and I_{ring} are the faradic disk and ring currents, respectively. N is the collection efficiency of the ring electrode, which is determined to be 0.43 herein.

The specific kinetic current density was calculated from the K-L equation:

$$J_k = \frac{J_L \times J}{J_L - J} \quad (6)$$

The electrochemical double layer capacitances (C_{dl}) of catalysts were measured by using a simple CV method. It is known that the C_{dl} value is expected to be linearly proportional to the electrochemically active surface area of the electrode. A potential range of 1.065-1.165 V vs. RHE was selected for the capacitance measurements. Then, the capacitive currents of ΔJ @1.11 V/2 were plotted as a function of the CV scan rate of 2, 4, 6, 8 and 10 mV s^{-1}. These data were fit to a line, the slope of which is the geometric C_{dl}.

The steady-state i-t chronoamperometric response was tested at a polarizing potential of 0.7 V versus RHE in the O_2-saturated electrolyte, and 3 M methanol was introduced into the 65 mL electrolyte to examine methanol poisoning. For comparison, the

commercial Pt/C catalyst with Pt loading of 20 wt% (Johnson Matthey, Pt particle size: 2-5 nm) were also used as the benchmarking catalysts for the ORR, and the same procedure as described above was used to conduct the electrochemical measurement; the Pt loadings were 20 μg_{Pt} cm^{-2} for the commercial Pt/C catalyst.

The measurements of rechargeable zinc-air batteries were performed on home-built electrochemical cells. All data were collected from the as-fabricated cell with a CHI 760E (CH Instruments, Inc., Shanghai, China) electrochemical workstation at room temperature. Briefly, zinc foil was used as the anode, and catalysts loaded on 1.5 cm × 5 cm nickel foam (catalyst loading amount of 1.0 mg cm^{-2}) were used as the air cathode. For comparison, the primary battery was also made from Pt/C. The electrolyte was a mixture solution of 6.0 M KOH and 0.2 M zinc acetate. These galvanostatic discharge curves were recorded using a LAND battery testing station (CT2001A) at room temperature. Polarization data were collected using the LSV method at a scan rate of 5 mV s^{-1} with cut-off voltages of 0.4 V for the discharge curves at 25 °C with CHI 760E electrochemical working station.

Computational Method

All the density functional theory (DFT) calculations were performed by Vienna Ab-initio Simulation Package (VASP), [2,3] employing the Projected Augmented Wave (PAW) method. [4] The revised Perdew-Burke-Ernzerhof (RPBE) functional was used to describe the exchange and correlation effects.[5-7] The GGA + U calculations are performed using the model proposed by Dudarev et al, [8] with the U_{eff} (U_{eff} = Coulomb U – exchange J) values of 5 eV for Mo. For all the geometry optimizations, the cutoff energy was set to be 450 eV. A 4×2×1 Monkhorst-Pack grids was used to carry out the surface calculations on MoO_2 and MoO_2@Co. [9] The MoO_2@Co structure was modelled as one Co_4 cluster on the (001) surface of MoO_2. At least 20 Å vacuum layer was applied in z-direction of the slab models, preventing the vertical interactions between slabs.

In alkaline conditions, OER could occur in the following four elementary steps:

$$OH^- + * \rightarrow {}^*OH + e^-$$

$${}^*OH + OH^- \rightarrow {}^*O + H_2O + e^-$$

$${}^*O + OH^- \rightarrow {}^*OOH + e^-$$

$^{*}OOH + OH^{-} \rightarrow * + O_2 + H_2O + e^{-}$

where * denotes the active sites on the catalyst surface. The ORR is considered as the reverse reaction of OER. Based on the above mechanism, the free energy of three intermediate states, *OH, *O, and *OOH, are important to identify a given material's OER and ORR activity. The computational hydrogen electrode (CHE) model [10] was used to calculate the free energies of OER and ORR, based on which the free energy of an adsorbed species is defined as

$\Delta G_{ads} = \Delta E_{ads} + \Delta E_{ZPE} - T\Delta S_{ads}$

where ΔE_{ads} is the electronic adsorption energy, ΔE_{ZPE} is the zero point energy difference between adsorbed and gaseous species, and $T\Delta S_{ads}$ is the corresponding entropy difference between these two states. The electronic binding energy is referenced as ½ H_2 for each H atom, and (H_2O – H_2) for each O atom, plus the energy of the clean slab. The corrections of zero point energy and entropy of the OER and ORR intermediates can be found in the supporting information.

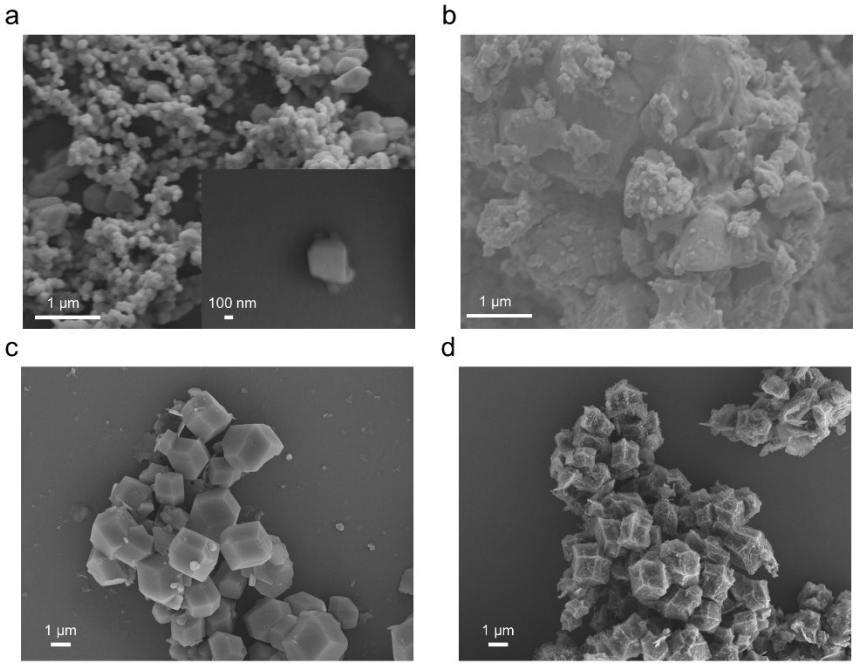

Figure S1 SEM images of the (a) customized Mo-MOFs and (b) its pyrolysis product; (c) Mo-MOF @ BIMZIF and its resultant (d) Co-MoO_2-NC-900.

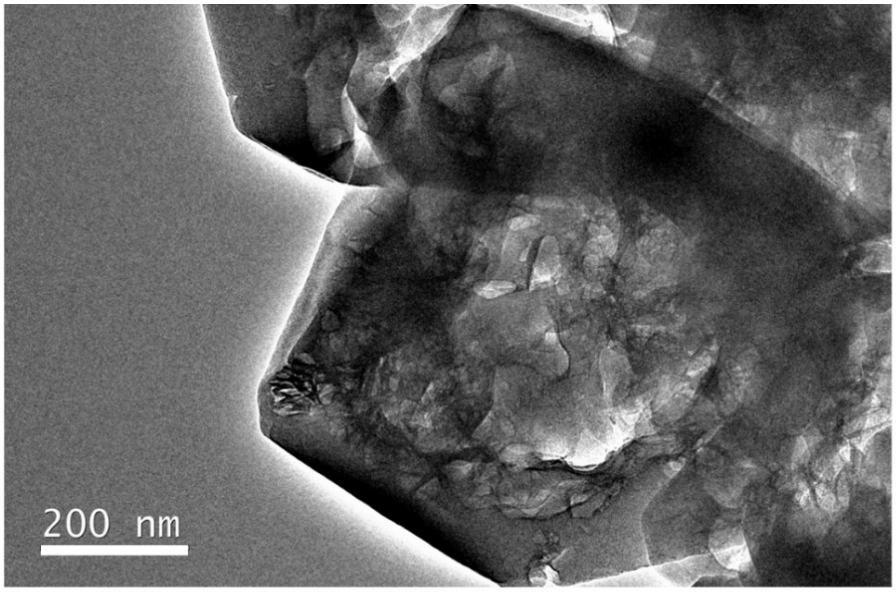

Figure S2 TEM image of core-shell Mo-MOF@BIMZIF.

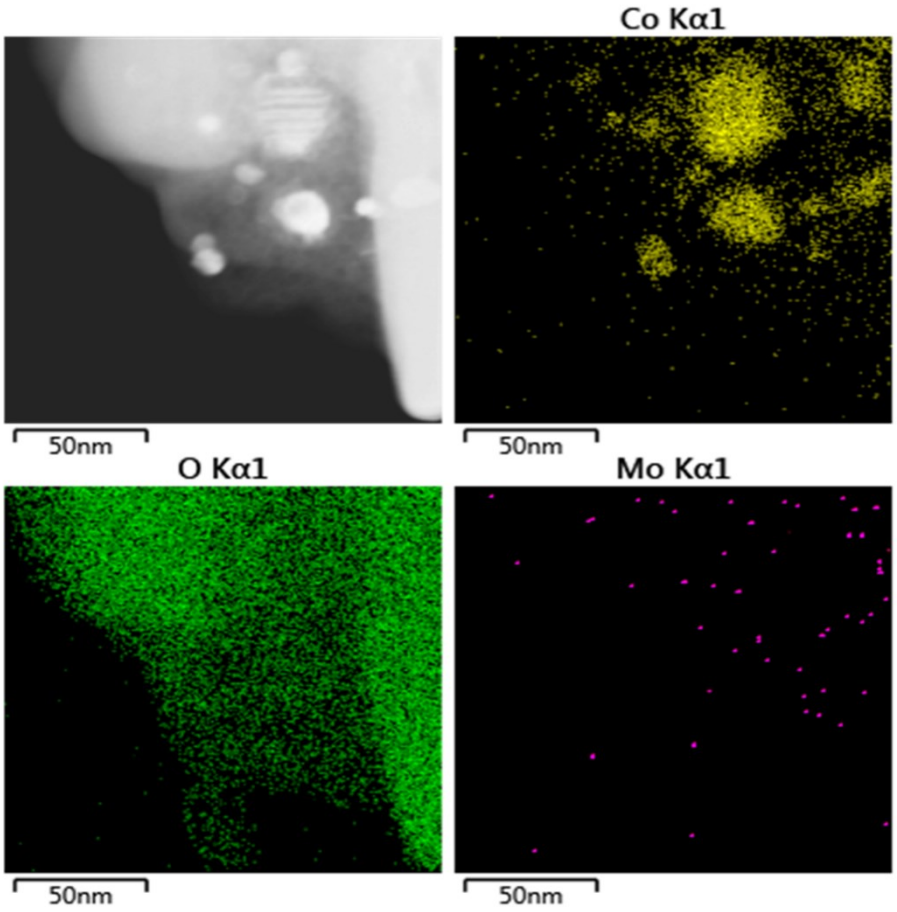

Figure S3 TEM image and EDS mapping of Co-MoO_2-NC-900 showing O species coexists with the cobalt nanoparticle across the CNTs.

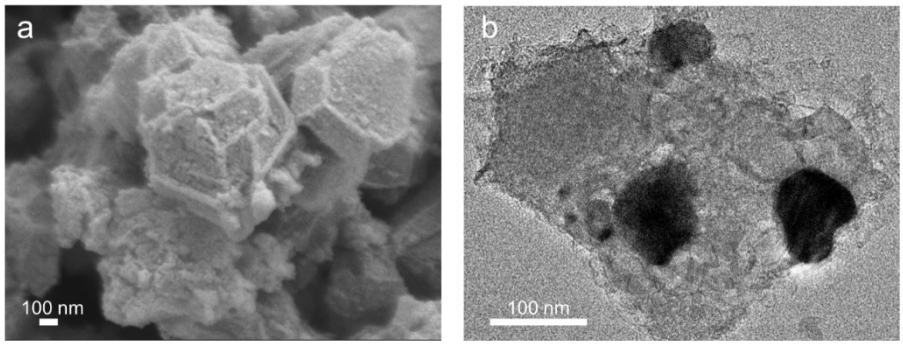

Figure S4 SEM (a) and TEM (b) images of Co-MoO_2-NC-800.

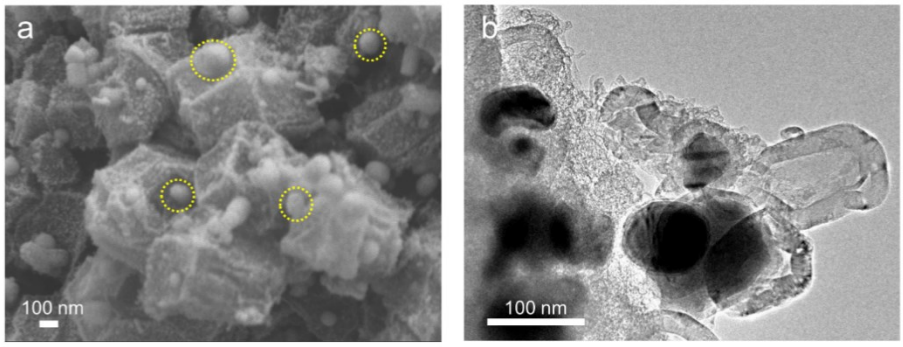

Figure S5 (a) SEM and (b) TEM images of Co-MoO_2-NC-1000.

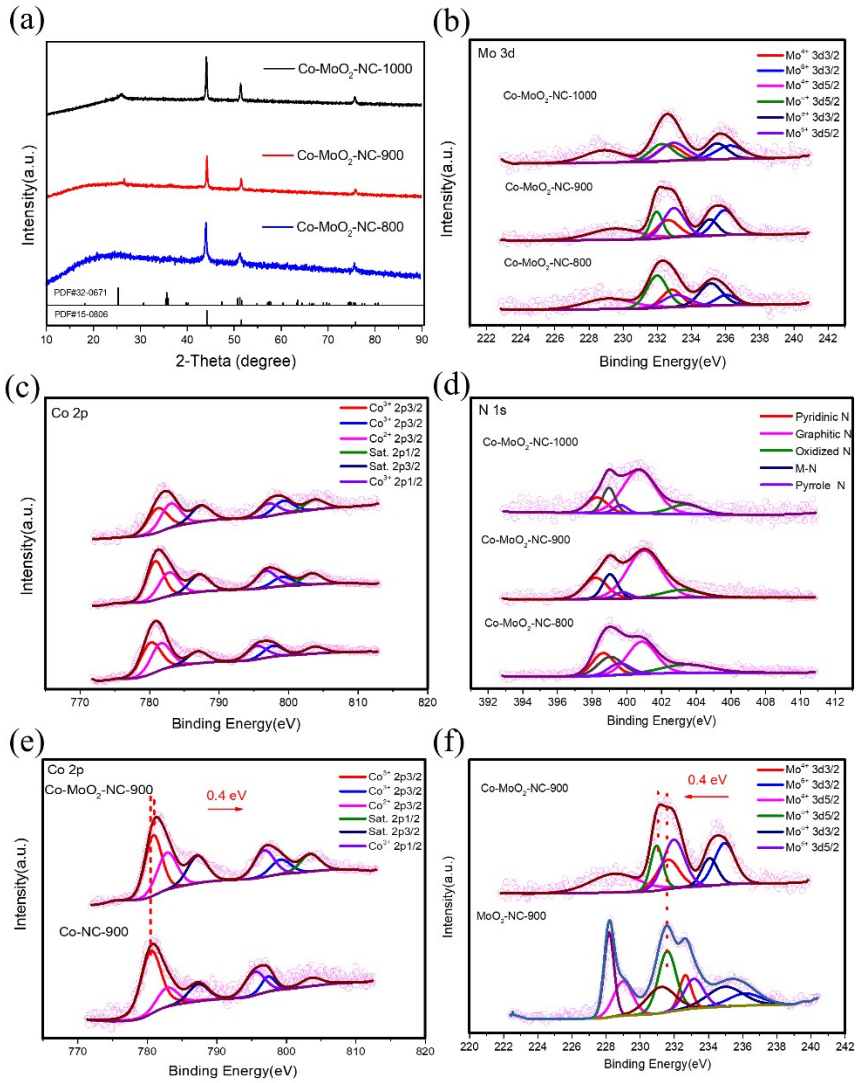

Figure S6 The Chemical phase, surface chemical state of Co-MoO_2-NC samples. (a) PXRD pattern; (b) Mo 3d, (c) Co 2p and (d) N 1s XPS spectra; XPS survey spectra of (e) Co-NC-900 and Co-MoO_2-NC-900 , and (f) MoO_2-NC and Co-MoO_2-NC-900.

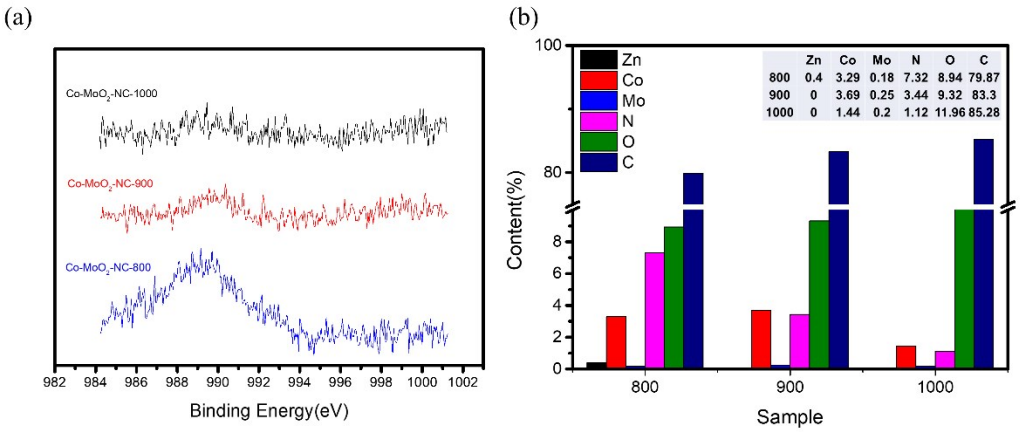

Figure S7 (a) Zn 2p spectrum of and (b) metal content of Co-MoO_2-NC products.

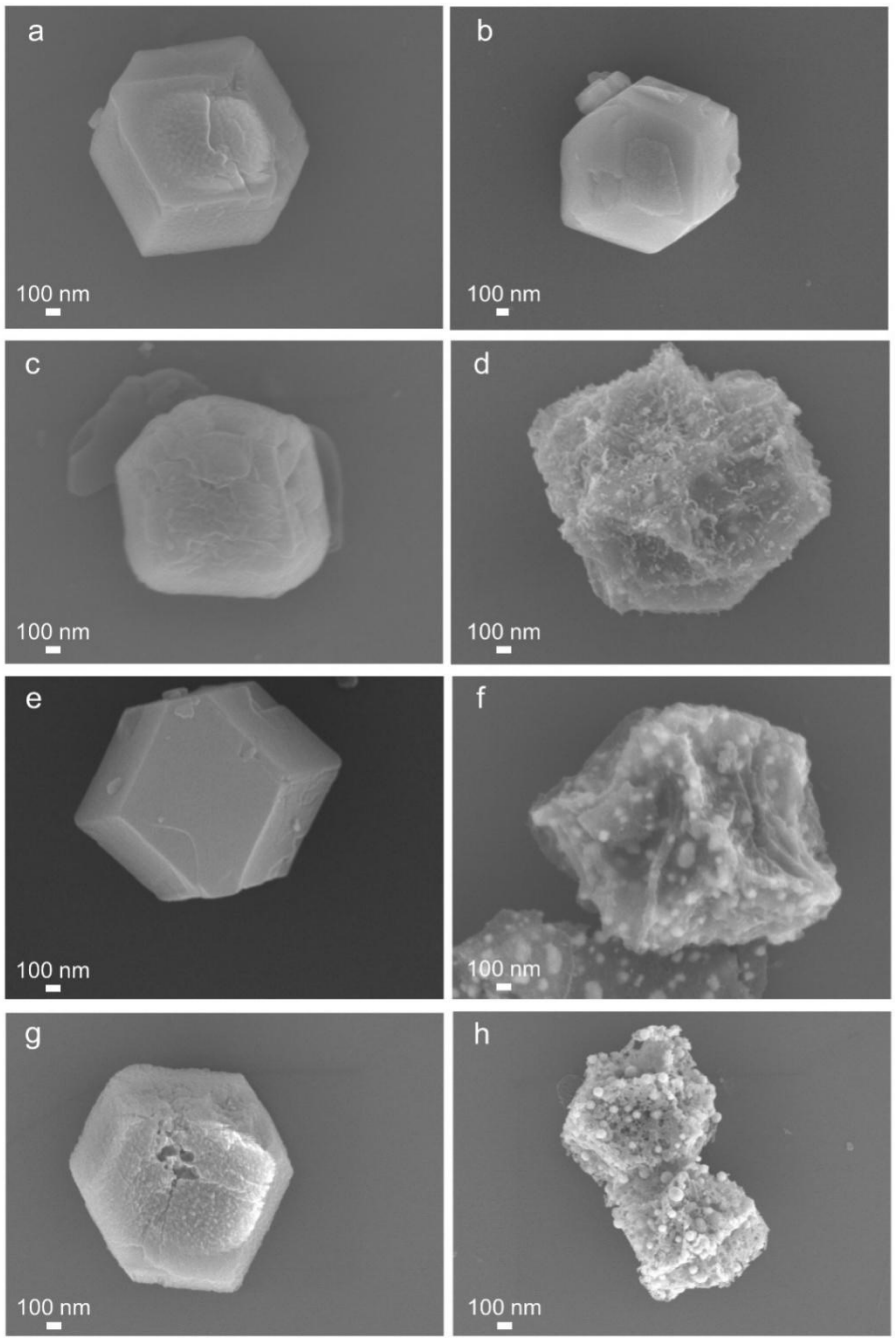

Figure S8 SEM images of (a, b) Mo-MOF @ BIMZIF-Co/Zn-0:3 and its resultant, (c, d) Mo-MOF @ BIMZIF-Co/Zn-1:2 and its resultant, (e, f) Mo-MOF @ BIMZIF-Co/Zn-2:1 and its resultant and (g, h) Mo-MOF @ BIMZIF-Co/Zn-3:0 and its resultant.

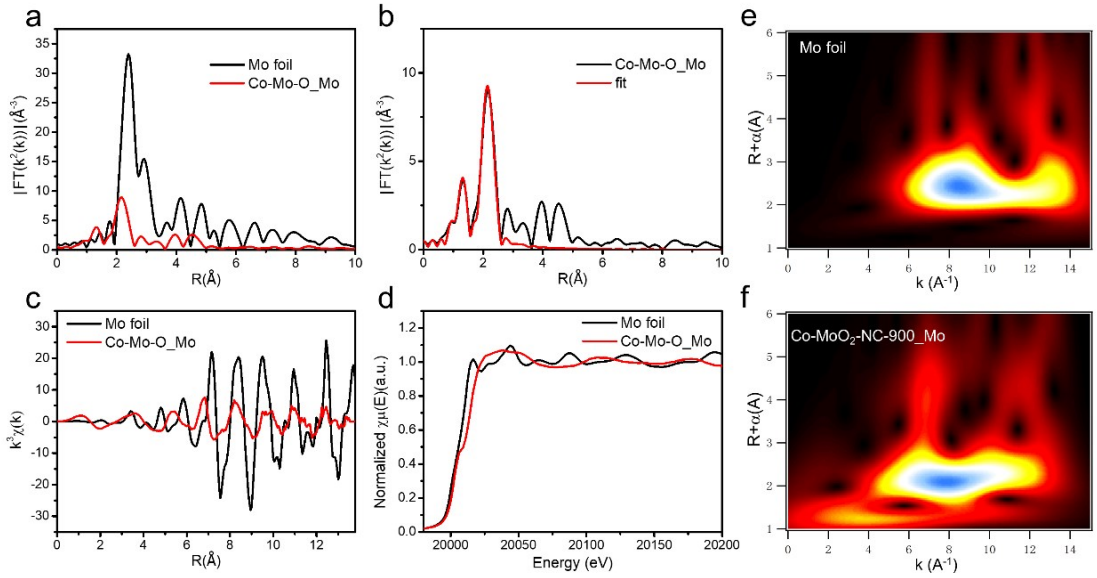

Figure S9 (a) K-edge EXAFS spectra of Co-MoO_2-NC-900_Mo and Mo foil. (b) Experimental and best-fitted EXAFS spectra in R space for Co-MoO_2-NC-900_Mo. (c) Experimental and best-fitted EXAFS spectra in K space for Co-MoO_2-NC-900_Mo. (d) Experimental XANES spectra for Co-MoO_2-NC-900_Mo and Mo foil. (e) WT for the k3-weighted EXAFS signals for Mo foil and (f) Co-MoO_2-NC-900_Mo.

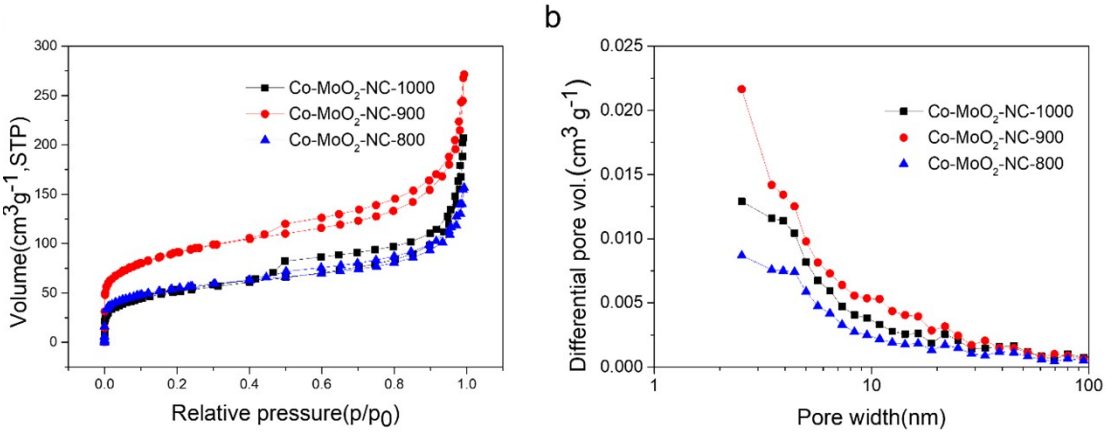

Figure S10 (a) N_2 sorption isotherms and (b) corresponding pore size of Co-MoO_2-NC samples.

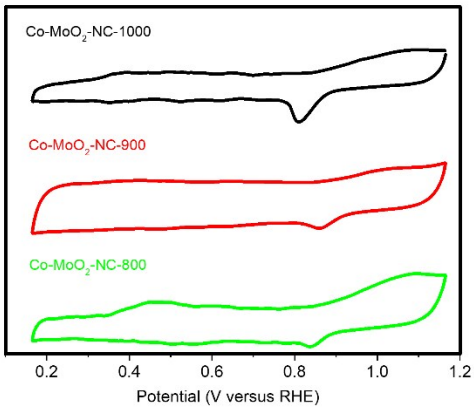

Figure S11 CV curves of Co-MoO_2-NC-800, 900, 1000.

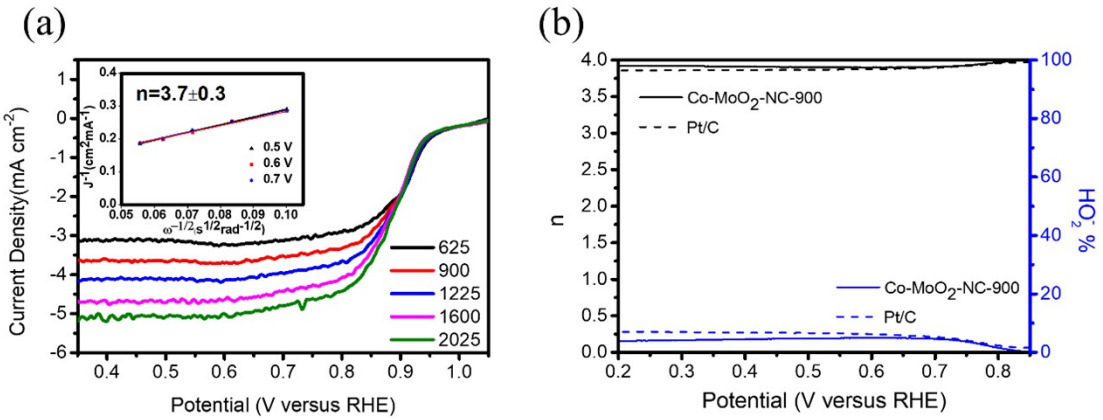

Figure S12 (a) LSV curves of Co-MoO_2-NC-900 catalyst, and transfer number (n), (b) percentage of peroxide in the total oxygen reduction products and the number of electron transfer at the Co-MoO_2-NC-900 and Pt/C electrodes based on the RRDE result.

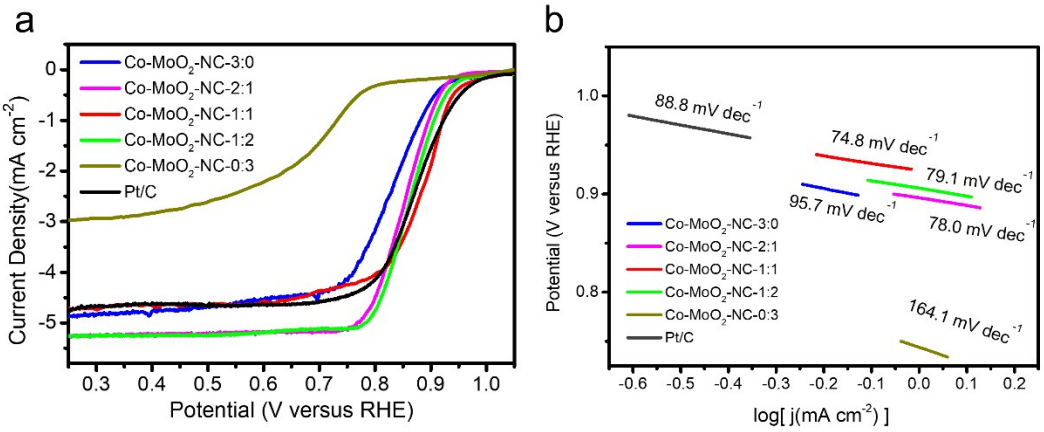

Figure S13 (a) ORR polarization curves of in O_2-saturated 0.1 M KOH at 1600 rpm and (b) Tafel plots for ORR of Co-MoO_2-NC products with different Co/Zn ratio (Co-

MoO_2-NC-1:1 is Co-MoO_2-NC-900 sample).

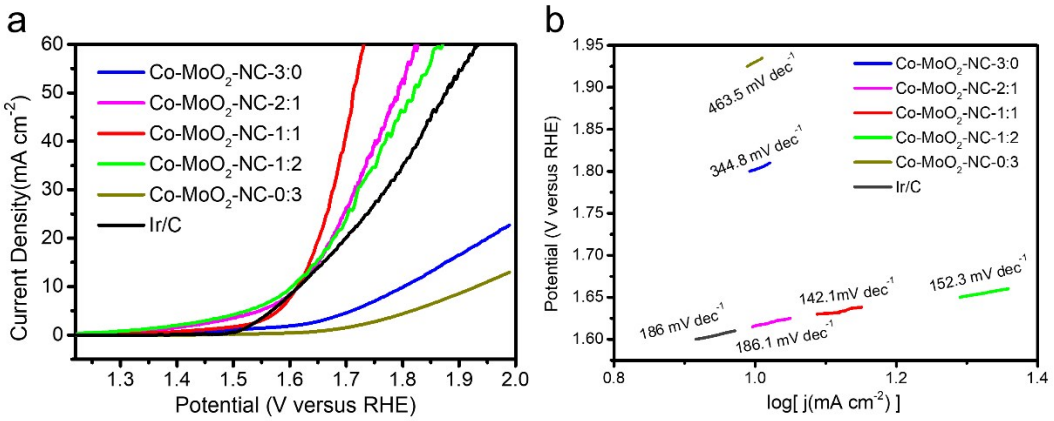

Figure S14 (a) OER polarization curves of in O_2-saturated 0.1 M KOH at 1600 rpm and (b) Tafel plots for OER of Co-MoO_2-NC products with different Co/Zn ratios (Co-MoO_2-NC-1:1 is Co-MoO_2-NC-900 sample).

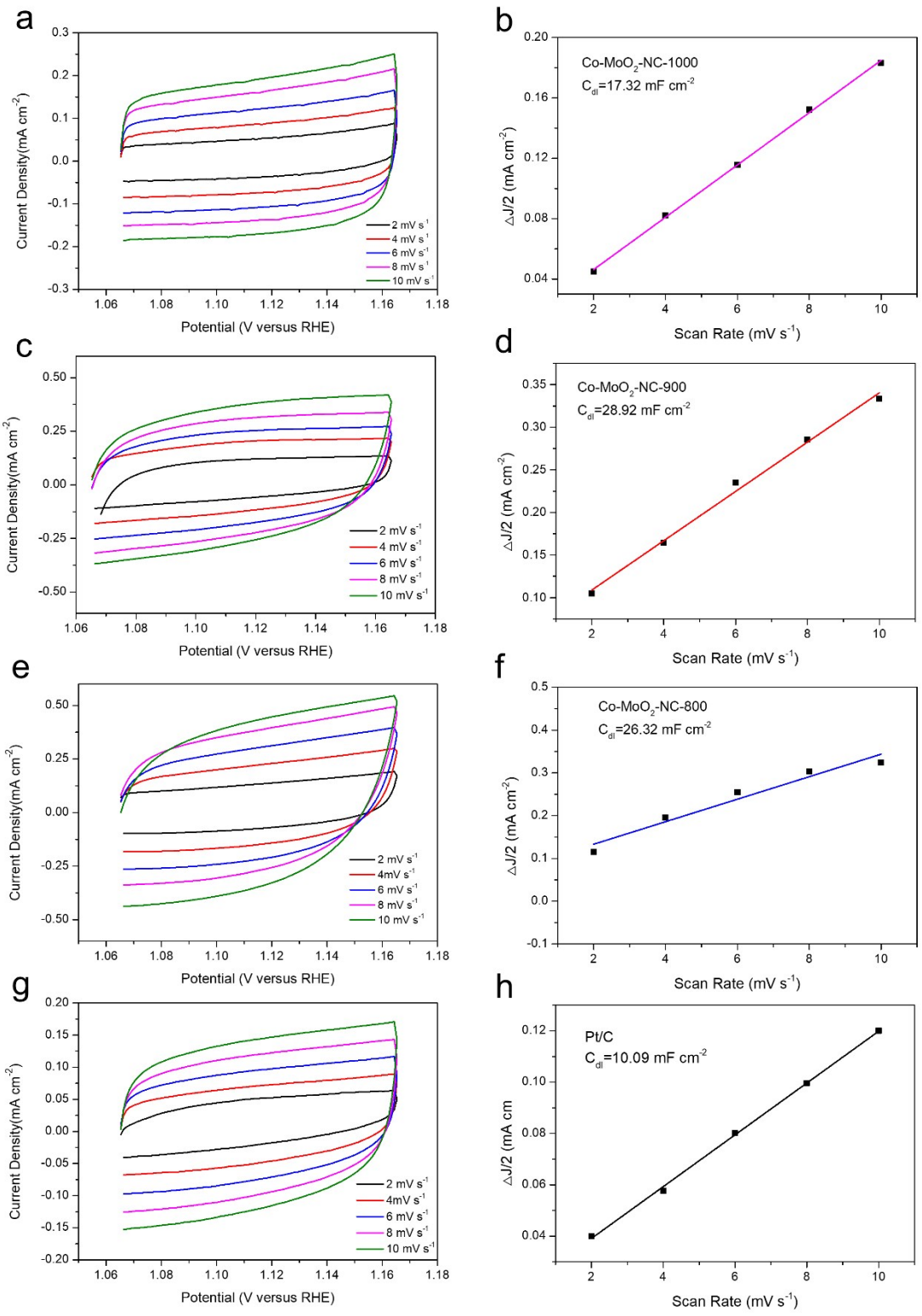

Figure S15 Cyclic voltammograms in the region of 1.065-1.165 V vs. RHE at various scan rates and the corresponding linear fitting of the capacitive currents vs. scan rates to estimate the C_{dl}. (a) and (b) for Co-MoO_2-NC-1000; (c) and (d) for Co-MoO_2-NC-900 ;(e) and (f) for Co-MoO_2-NC-800; (g) and (h) for Pt/C and the calculated C_{dl} values are shown in the insets.

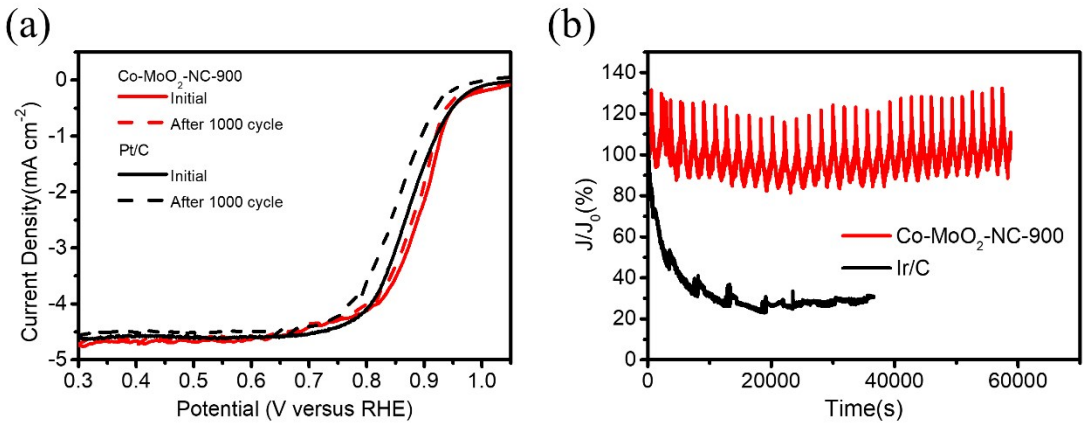

Figure S16 (a) LSV curves before and after 1000 potential cycles for ORR; (b) i–t cures at 1.5 V for 60000 s.

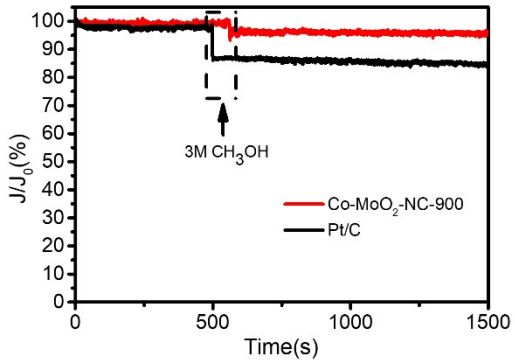

Figure S17 The i-t curves at 0.5 V after the introduction of 3 M methanol into 65 mL of 0.1 M KOH solution for Co-N-PHCNTs and Pt/C.

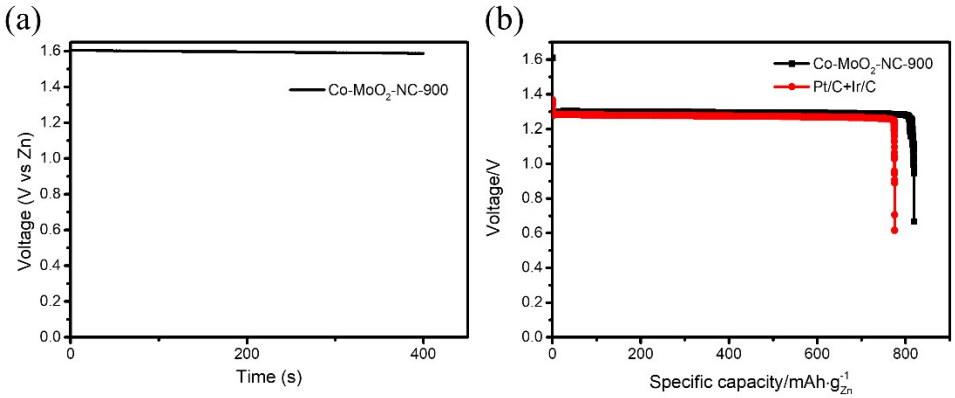

Figure S18 (a) Open-circuit plots of Co-MoO_2-NC-900 and (b) specific capacities normalized to the mass of consumed zinc in batteries at 5 mA cm^{-2} of Zn–air batteries driven by Co-MoO_2-NC-900 and Pt/C+Ir/C.

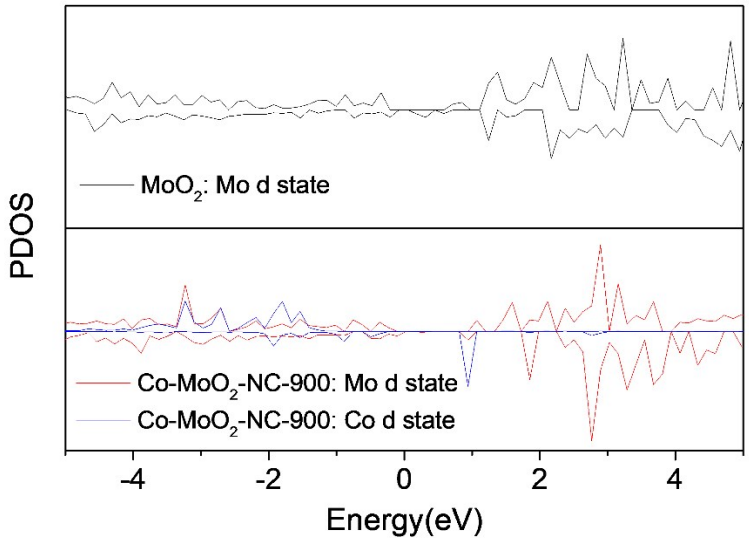

Figure S19 PDOS of Co-MoO_2-NC-900 and MoO_2

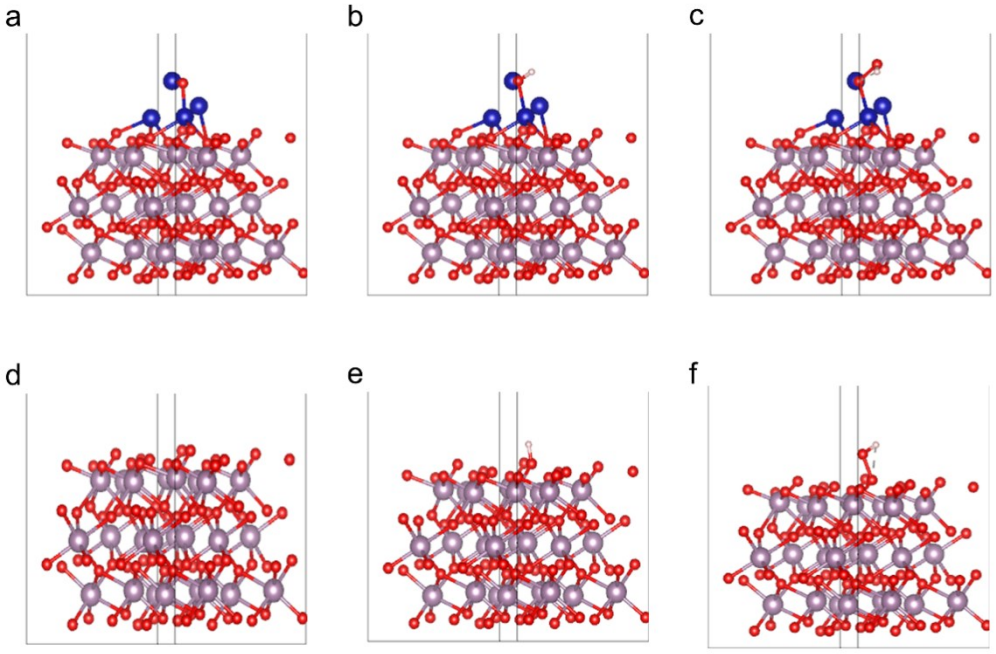

Figure S20 Simulation module of (a) Co-MoO_2-NC-900--O, (b) Co-MoO_2-NC-900—OH and (c) Co-MoO_2-NC-900—OOH;(d) MoO_2--O, (e) MoO_2—OH and (f) MoO_2—OOH.

Table S1 EXAFS fitting parameters at the Co/Mo K-edge for various samples

Sample	Shell	N [a]	R (Å) [b]	σ^2 (Å$^2\cdot10^3$) [c]	$\Delta E0$ (eV) [d]	R factor (%)
Co-MoO_2-NC-900-Mo	Mo-O	1.2	1.75	3.4	14.2	1.0
	Mo-Co	2.9	2.54	5.7	3.0	
Co-MoO_2-NC-900-Co	Co-Co	10.1	2.50	6.7	7.7	0.1

[a] N: coordination numbers; [b] R: bond distance; [c] σ^2: Debye-Waller factors; [d] ΔE_0: the inner potential correction. R factor: goodness of fit. $S02$ were set as 0.85/0.9 for Co-Co/(Mo-O/Mo-Co), which were obtained from the experimental EXAFS fit of Cofoil/Mofoil reference by fixing CN as the known crystallographic value and was fixed to all the samples.

Note: The error range of N and σ^2 is 20%, and the accuracy range of R is +-0.03A.

Table S2 The electrochemical properties of as-prepared electrocatalysts and the reference (Pt/C and Ir/C)

Electroatalyst	$E_{j=10}$ (V)	$E_{1/2}$(V)	E_{onset}(V)	ΔE ($E_{j=10}$ - $E_{1/2}$) (V)	$J_{k\ at\ 0.85V}$(mA cm^{-2})
Co-MoO_2-NC-3:0	1.802	0.83	0.96	0.972	3.1
Co-MoO_2-NC-2:1	1.655	0.85	0.97	0.805	5.8
Co-MoO_2-NC-900 (1:1)	1.600	0.89	0.99	0.71	26.0
Co-MoO_2-NC-1:2	1.633	0.86	0.97	0.773	7.5
Co-MoO_2-NC-0:3	1.930	0.71	0.81	1.22	0.47
Co-MoO_2-NC-800	1.654	0.85	0.96	0.804	21.7
Co-MoO2-NC-1000	1.791	0.82	0.94	0.971	20.6
Ir/C and Pt/C	1.618(for Ir/C)	0.87 (for Pt/C)	1.00 (for Pt/C)	0.748	7.7(for Pt/C)

Table S3 The catalytic performance of various bifunctional electrocatalysts from literatures.

Literature	electrocatalyst	ORR		OER	ΔE
		E_{onset} (V)	$E_{1/2}$ (V)	$E_{j=10}$ (V)	($E_{j=10}$ - $E_{1/2}$) (V)
This work	Co-MoO_2-NC-900	0.99	0.89	1.600	0.71
This work	Ir/C-Pt/C	1.00 (Pt/C)	0.87 (Pt/C)	1.618(Ir/C)	0.748
J. Am. Chem. Soc. 2016, 138, 10226-10231.	Co_4N/CNW/CC	0.89	0.80	1.50	0.74
Adv. Mater. 2017, 29, 1704117.	NC-Co_3O_4-90	0.91	0.87	1.59	0.72
Nat.Mater. 2011, 10, 780-786	C-MOF-C2-900	0.92	0.817	1.58	0.763
Adv. Energy Mater. 2018, 8, 1802263	$CoIn_2S_4$/S-rGO	0.93	0.82	1.6	0.78
Nat. Energy 2016,1, 15006	N-GRW	0.92	0.84	1.59	0.75
Energy Environ.Sci. 2016, 9, 2020-2024	NiFe-LDH- Fe-N-C	N/A	N/A	N/A	0.75
Sci. Adv. 2016, 2, 1501122	N-GRW	0.92	0.84	1.59	0.75
Adv. Energy Mater. 2018, 8, 1801495	rGO/CB_2/Co-Bi	0.88	0.7	1.58	0.87
Adv. Energy Mater. 2018, 8, 1703539	DN-CP@G	N/A	0.801	1.788	0.987
Adv. Mater. 2016, 28, 3000-3006	NCNF-1000	0.97	0.82	1.84	1.02
Adv. Energy Mater. 2017, 7, 1602420	N-GCNT/FeCo-3	1.03	0.92	1.73	0.81

Table S4 A survey of the performance of rechargeable Zn-air batteries with various electrocatalysts.

Literature	electrocatalyst	Peak power density (mW cm^{-2})	Stability
This work	**Co-MoO_2-NC-900**	**176.5**	**over 2000 cycles of 677 h at 5 mA cm^{-2}**
Adv. Energy Mater. 2017, 1602420	NGCNT/ FeCo	89.3	N/A
Adv. Funct. Mater. 2017, 7, 1705048	Co-N-CNTs	101	130 cycles of 15 h at 2 mA cm^{-2}
Adv. Energy Mater. 2018, 8, 1800612.	CMO/S-300	152	120 cycles of 13 h at 5 mA cm^{-2}
Adv. Energy Mater. 2018, 8, 1802263	$CoIn_2S_4$/S-rGO	133	150 cycles of 50 h at 10 mA cm^{-2}
Adv. Funct. Mater. 2018, 28, 1704638	Co–Nx/C NRA	193.2	80 h at 50 mA cm^{-2}
Energy Environ. Sci. 2017, 10, 742-749.	1100-CNS	151	300 cycles of 55 h at 10 mA cm^{-2}
Adv. Energy Mater. 2018, 8, 1800480	CoNi@NCNT/NF	127	N/A
Adv. Energy Mater. 2018, 8, 1703539	DN-CP@G	135	250 cycles of 250 h at 5 mA cm^{-2}

Table S5 The correction of zero point energy and entropy of the adsorbed and gaseous species.

	ZPE(eV)	TS(eV)
*OOH	0.35	0
*O	0.05	0
*OH	0.31	0.01
H_2O	0.56	0.67
H_2	0.27	0.41

References

1. X. Shi, A. Wu, H. Yan, L. Zhang, C. Tian, L. Wang and H. Fu, *J. Mater. Chem. A*, 2018, **6**, 20100-20109.
2. G. Kresse and J. Furthmüller, *Phys. Rev. B*, 1996, **54**, 11169-11186.
3. G. Kresse and J. Hafner, *Phys. Rev. B*, 1994, **49**, 14251-14269.
4. P. E. Blöchl, *Phys. Rev. B*, 1994, **50**, 17953-17979.
5. J. P. Perdew, K. Burke and M. Ernzerhof, *Phys. Rev. Lett.*, 1996, **77**, 3865-3868.
6. Y. Zhang and W. Yang, *Physical Review Letters*, 1998, **80**, 890-890.
7. B. Hammer, L. B. Hansen and J. K. Nørskov, *Phys. Rev. B*, 1999, **59**, 7413-7421.
8. S. L. Dudarev, G. A. Botton, S. Y. Savrasov, C. J. Humphreys and A. P. Sutton, *Phys. Rev. B*, 1998, **57**, 1505-1509.
9. H. J. Monkhorst and J. D. Pack, *Phys. Rev. B*, 1976, **13**, 5188-5192.
10. J. K. Nørskov, J. Rossmeisl, A. Logadottir, L. Lindqvist, J. R. Kitchin, T. Bligaard and H. Jónsson, *J. Phys. Chem. B*, 2004, **108**, 17886-17892.